Cause of Pulse Artefacts Inherent to the Electrodes of Neuromodulation Implants

Peter Single and Jonathan Scott, *Senior Member, IEEE*

***Abstract*—The current pulses delivered through platinum electrodes by medical implants to recruit neurones give rise to slowly-decaying voltage tails, called "artefacts". These tails make measurement of evoked potentials following the pulses very difficult. We present evidence to show that in a typical clinical scenario these tails are mostly caused by concentration gradients of species induced in the electrical double layer adsorbed onto the surface of both stimulating and passive electrodes. A compact model is presented that allows simulation of these artefacts. The model is verified against measurements made in saline. This shows that electrode artefacts are an intrinsic property of the conductive electrodes of a lead.**

***Index Terms*—Biomedical electrodes, electrical stimulation, neuromodulation, compact model.**

I. Introduction

CONSIDERABLE interest has arisen recently in sensing neural activity in the presence of, and quickly following, neural stimulus pulses in order to apply feedback in neuromodulation systems [1]–[3]. The evoked compound action potentials (ECAP) synchronised with the stimulus and measured near the stimulation site betray the extent of neural recruitment resulting from the pulse. Measured ECAP can be of use both during the implantation surgery and for automatic adjustment of the stimulus pulse amplitude and locale in routine use.

Unfortunately, the stimulus pulses give rise to slowly-decaying voltage tails, cumulatively referred to as "artefacts". A typical neuromodulation pulse has an amplitude of several volts, while the amplitude of the signal visible at an electrode as a result of a nerve firing may be only a few microvolts. To be useful, the evoked responses must be recorded starting within about a hundred microseconds of the end of the stimulus pulse. The artefact tails have long been known to have amplitudes between millivolts and tens of microvolts depending upon the spacing between the stimulus and recording electrodes [4]. Considerable ongoing work addresses the difficulty of eliminating the artefact from captured signals, see for example [5]. Better-positioned sensor electrodes have greater artefact; this is because the ECAP disperses as it propagates from the recruitment site, and thus it is better to sense close to the recruitment site. It is demanding to design amplifiers capable of processing these signals for analog-to-digital conversion, particularly in integrated CMOS technology [6].

A compact model of the impedance of the electrode-electrolyte interface has been presented in [7]. This model uses Constant-Phase Elements (CPEs) amongst other more common elements in an equivalent-circuit representation of the interface between electrode and electrolyte. The model is able to accurately represent the impedance of the interface [8]. In a circuit simulator the model allows prediction of the residual voltage and artefact tails in some circumstances, but not all. As will be seen below, the model predicts zero artefacts in certain circuit configurations, but measurement reveals significant artefacts. It is clear that there is a mechanism at work that is not captured by the single-CPE compact model of [7].

Manuscript received October, 2017.

Peter Single is with Saluda Medical, Artarmon, Sydney, Australia. Jonathan Scott is with the School of Engineering, The University of Waikato, Hamilton 3240, New Zealand (email: jonathan.scott@waikato.ac.nz).

II. Split-Electrode Model

It has been hypothesized that the artefact can arise not only through residual charge left in the double layer surrounding an electrode after it conducts a current, but also by virtue of an uneven distribution of that charge along the surface of an electrode [9]. Such an uneven charge distribution can arise even without any net current flowing through the electrode into the electronics. One might visualise counter-charges in the diffuse region of the electrical double layer piling up at one end of an electrode as a result of surface conduction that in turn arises from fields generated by the stimulating electrodes [10]. Although [10] wisely proffers the comment that "for most purposes a more elaborate model is necessary", this idea of charges piling up at one end of an electrode suggests a straightforward way that a compact model might be constructed to simulate the phenomenon.

The electrode is split into multiple sections or "slices" that are modelled separately. The single-branch model of an electrode is replaced with one having n branches, each contributing $\frac{1}{n}$ times the total admittance (area) presented by the original electrode. The branches are joined together at a single node at the metal side of the electrode, but are connected only through the resistor mesh representing the bulk fluid on the fluid side of the interface.

As in [7], a rotationally-symmetric situation is considered, so that simulation is straightforward using a two-dimentional representation, and comparative measurements can be made with a cylindrical, implantable, platinum electrode array such as an octrode [11] or dodecatrode [12]. A typical lead with a set of electrodes (cylindrical platinum cuffs in this case) is pictured in figure 1. The equivalent circuit of a single cuff, omitting the diodes and memristors for clarity, is shown in figure 2. For small-signal simulations of scenarios that are safe for use in humans, the diode-memristor branch elements can be ignored. Nevertheless, the diodes at least must be included to detect and model Faradaic (nonlinear) effects [8]. Base

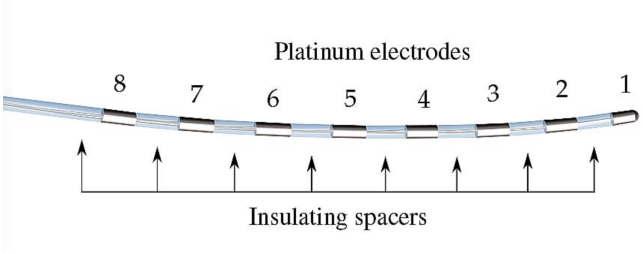

Fig. 1. An 8-element implantable electrode array. Each cuff is about 1.3 mm in diameter and 3 mm long, spaced by 4 mm insulating sections.

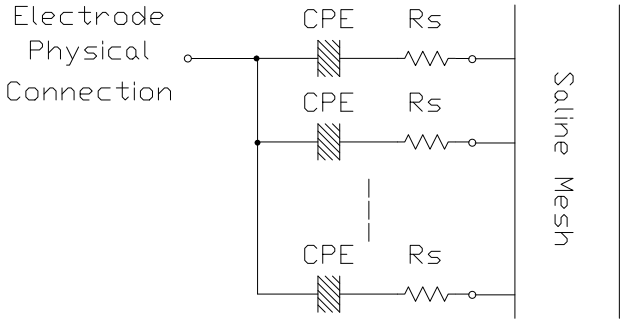

Fig. 2. The equivalent circuit of a single 3 mm cuff of an electrode array becomes a sequence of n parts each with its own CPE, and each tapping into different geometrical points in the mesh of resistors representing the electrolyte. The diodes are omitted for clarity, but must be included except for small-signal simulations.

model parameters for the CPE used in the circuit were taken from [8], trimmed to show agreement with the impedance observed looking into electrodes 1 and 2, and scaled according to the split factor in use. Our simulations use base values of CPE fraction $m = 1.5$, magnitude $|Z| = 6500\Omega$ at 1 Hz, and series resistance $R_S = 12\Omega$. The SPICE equivalent network was generated using a density of $k = 1.3$ from 10 mHz to 500 kHz. Resistor mesh values are calculated as described in [7] using a measured value of saline conductivity of 6400 Ωmm and on a grid selected to suit the split factor. The interested reader is referred to [7] for the involved definitions of these parameters.

In this manuscript we will chiefly consider one particular circuit arrangement. Stimulation current is applied to the second cylindrical cuff of the lead. The current return will be via the first cuff. The voltage of interest is that appearing between the fourth and seventh cuffs. This represents a typical, clinically-desirable arrangement for use in a feedback implant. The stimulus pulse will be a so-called biphasic pulse consisting of +5mA delivered for 240μs, zero current for 200μs, -5mA delivered for 240μs, and finally disconnection of the drive electronics. The form of the stimulus pulse is not particularly germane to the issue of how artefact arises.

This configuration was simulated using a single-CPE model for the electrodes in 0.1x Phosphate Buffered Saline (PBS). In the case of the single-branch electrode model of [7], absolutely zero artefact is predicted to appear between electrodes 4 and 7, assuming there is no load presented to the electrodes by the electronics. That means absolutely no current flows into or out

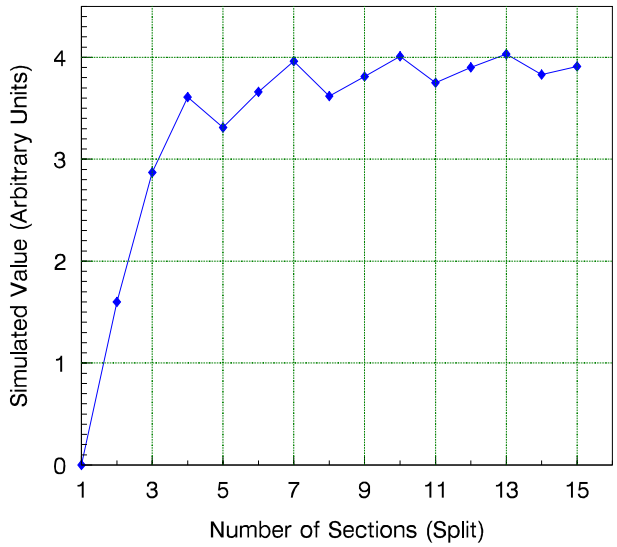

Fig. 3. Predicted artefact amplitude as a function of the number of sections into which an electrode cuff is split in the SPICE simulation. A split of 1 corresponds to using the original model of [7].

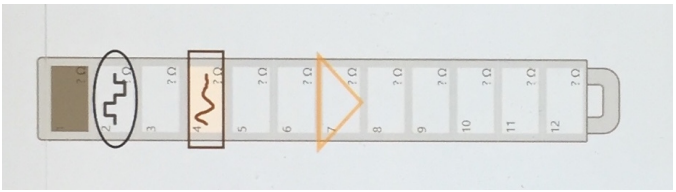

Fig. 4. Implanted Pulse Generator (IPG) wiring configuration as depicted on the screen of the controlling software. Stimulus is shown delivered to electrode 2 with ground return via electrode 1. Response is measured at electrode 4 with respect to electrode 7.

of any electrode apart from the stimulus current.[1] However, when the electrode model is split into ever-greater numbers of slices, the prediction changes. Figure 3 dramatically shows the impact. This would suggest that splitting the electrodes into 7 or more slices will be required to give reasonable accuracy. A split factor of $n = 11$ will be used in this work except where noted. Since the resistor mesh representing the electrolyte is also split into slices of the same geometric size, say $3/11^{ths}$ of a millimetre or finer, the number of nodes involved to simulate an electrode reaching over 60 mm of electrolyte can become quite large. SPICE takes from a few seconds to a few minutes to run a simulation on a typical personal computer.

III. Comparison with Measurement

A Saluda Medical "Evoke" implant was used to generate pulses and amplify the measured signals. The circuit wiring arrangement, discussed above, is depicted in figure 4 using an image taken from the screen of the software used to control the implant. The 0.1x PBS was created using Medicago 09-2051-100 PBS tablets and de-ionised water at the rate of 1 tablet

[1] We assume that FEAs and the driving current sources are effectively ideal. Large artefacts appear if this is not the case. Such externally-induced artefacts are well known, readily predicted, readily avoided, and not of interest here.

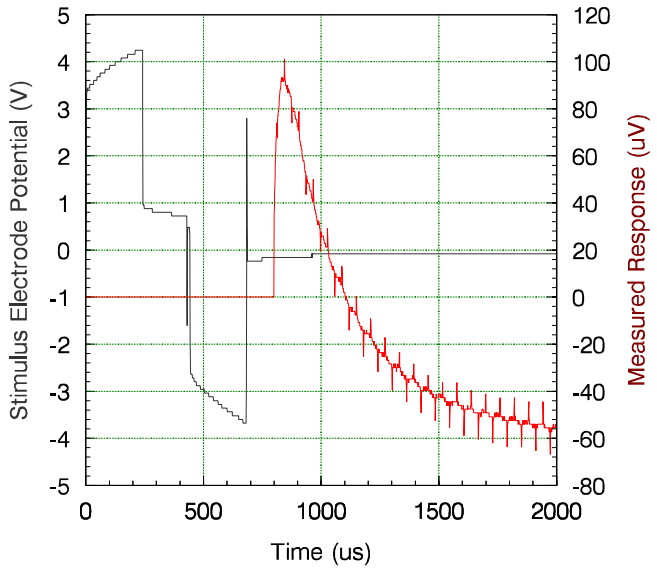

Fig. 5. Stimulus and response voltage waveforms with 5mA peak stimulation applied from the second to the first electrode and measuring the voltage present between the fourth and seventh electrodes, as depicted in figure 4. The response is blanked until about 800μs after the start of the stimulus. The series of small impulses on the received pulse tail are caused by the implant ADC operation and are not part of the signal.

per litre. This is a common phantom for tissue in cerebrospinal fluid (CSF). The received signal is digitised by the implant, but was also digitised using a Tektronix TPS2014 isolated-input oscilloscope from a test port provided by the implant IC. The same data can be obtained from the implant, but only at a lower sample rate of approximately 16,000 samples per second. There is an uncertain additive contribution from common-mode signals owing to the implant amplifier's finite Common-Mode Rejection Ratio (CMRR) that is no worse than 75dB.[2] Figure 5 shows the stimulus voltage and a typical measured response signal for a 5mA pulse. As can be observed in the figure, the front-end amplifier (FEA) is blanked during the pulse. The blanking released 800μs after the start of the pulse sequence, or approximately 100μs after the stimulus current switches off. An arbitrary dc offset has been subtracted from the test port voltage as the Implant Pulse Generator (IPG) FEA is ac coupled. The array of small spikes spaced about 31μs apart are clock feedthrough associated with the analog-to-digital conversion inside the implant chip and should be ignored. Substantial switching spikes are visible on the stimulus voltage trace in figure 5, especially at the end of the second pulse. These cause a contribution to the artefacts that does not vary with stimulus magnitude. As will be seen below this contributes a constant offset to the magnitude of the measured artefacts.

It proves difficult to obtain agreement between simulation and measurement. This difficulty is attributed to artefacts being the sum of several components that to a large degree cancel each other out. Thus small deviations in any one component, associated perhaps with a particular cuff (contact), can give rise to relatively large variation in final artefact value. We believe this accounts for the anecdotal observation that artefact is better or worse on different contacts, for no obvious reason. This variability manifests even in saline where the inhomogeneity of tissue is not an issue. The model presented here allows these components to be identified separately.

[2]The Evoke implant relies on on-chip capacitor matching to achieve its common mode rejection, rather than a tail current-source figure of merit. For this reason the sign of common-mode gain is unpredictable, some implants will exhibit superb CMRR, while others may be as low as 75dB.

A. Artefact from Passive (Unconnected) Electrodes

All the electrodes on a lead are exposed to a voltage gradient along their length during the pulse. Charge accumulates at one end of each conductive cuff compared to the other. There is generated a voltage gradient in the tissue or electrolyte in which the lead is immersed by the dipole of the stimulating and return electrodes, 2 and 1 in this example. Charge is more easily displaced along the surface of the cuff than the surrounding medium. Once the pulse is over, even an electrode that was never electrically connected, and conducted zero net current, acquires a charge imbalance along its surface that manifests itself as a transient net potential difference between the metal of the cuff and the bulk medium. Figure 6 shows a simplified circuit with 4 electrodes, each split into two slices. The CPEs of a single electrode become charged by the "circulating current". Figure 7 plots the potential resulting from accumulated charge on electrode 4 purely as a result of the stimulus current flowing between electrodes 2 and 1. Note that the distribution is not symmetrical. The simulation suggests that the average or net potential is around 100μV across electrode 4 from contact to the bulk saline. The residual potential is larger on individual electrodes that are closer to the stimulating pair and smaller on ones further away. This distribution relaxes at the end of the pulse as the charge redistributes.

The same mechanism operates on electrode 7, but less than 2μV results. Thus, a total of $\approx 100\mu$V contribution is made to V(4,7), the sensed voltage, chiefly because of the net voltage between the tissue side and the metallic side of electrode 4.

B. Artefact from Stimulation Electrodes

The stimulating electrode, number 2 in our example, develops around 25 times the charge gradient along the length of its surface compared with electrode 4, since one end of it is much closer to the ground return path than the other. Refer to figure 8. At the edge of this electrode, even a stimulus pulse of 5mA causes nonlinear effects, although much less nonlinear action would be expected if the current were to be delivered evenly across the area of the cuff. This large charge gradient relaxes at the end of the pulse, inducing potential differences between all the electrodes along the entire lead. The contribution to V(4,7) is $\approx 100\mu$V.

It should be noted that there is a large dc offset in the potential present along both stimulating electrodes, as visible for electrode 2 in figure 8. This dc offset produces no contribution to artefact, provided the current sources are close enough to ideal. This is the case in the implant we used for

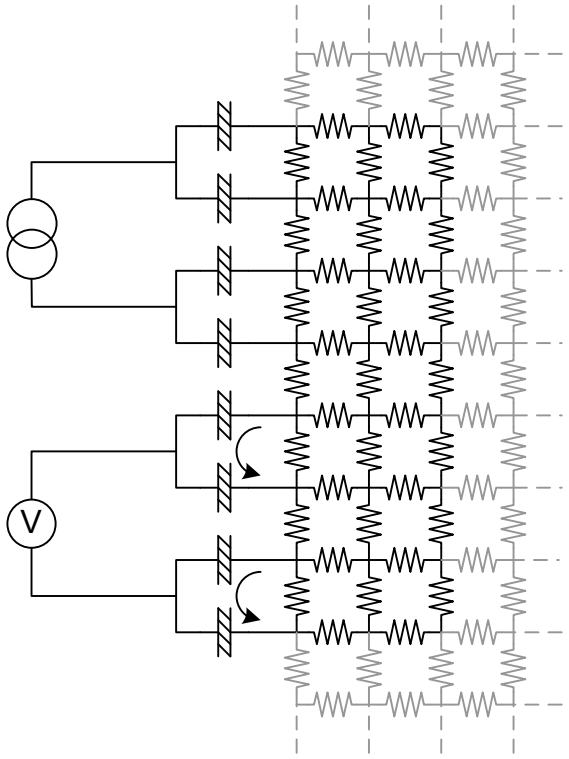

Fig. 6. Simplified circuit to assist in visualising the generation of artefacts in passive electrodes. Arrows show current induced by the stimulus in one end of a passive electrode and out of the other.

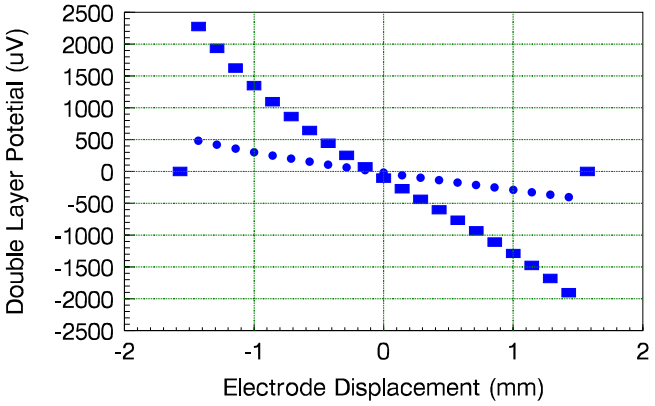

Fig. 7. Simulated potential resulting from accumulated charge in the interface layers as a function of position along electrode 4 as a result of the 5mA stimulus pulses applied between electrodes 2 and 1. The electrode was split into 21 slices. Rectangular symbols are voltage recorded at the end of the biphasic stimulus pulse depicted in figure 5. The dots represent data at 1ms elapsed time, showing the relaxation. The electrode was not connected, so net electrode current remains zero throughout.

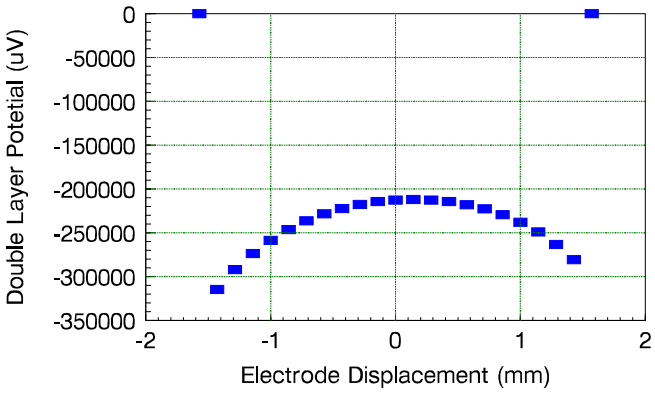

Fig. 8. Simulated potential resulting from accumulated charge in the interface layers as a function of position along electrode 2 as a result of the 5mA stimulus pulses. Data recorded at the end of the biphasic stimulus pulse depicted in figure 5. The y-axis units are chosen to be the same as those in figure 7.

measurement. Thus only the *gradient* in the electrode potential generates artefacts in out scenario. Were there to be some loading on any electrode, this might well introduce artefact via the average charge accumulated on an electrode. We are able to assume all loading to be negligible for this work.

The ground return electrode does the same as the stimulating electrode, but the polarity of its contribution is the reverse, and it is a different distance from the receiving pair. It also produces an artefact contribution to V(4,7). The difference between the contributions from the stimulating and ground electrodes is typically $\approx 50\mu$V at 5mA.

C. Common-Mode Artefact

The total charge accumulated across each of the stimulating and return electrodes between the metal and the medium (as different from the gradient along the cuff purely on the electrolyte side) is many hundreds of mV, as seen in figure 8. The circuit ground remains connected to the return current electrode. The average voltage across the ground electrode appears as a common-mode signal. This can give rise to as much as $\approx 50\mu$V of additional artefact amplitude given the CMRR of the FEAs.

D. Summed Artefact

Finally it is possible to address the question of what total artefact will be generated at the receiving electrodes by these mechanisms operating together. Figure 9 shows artefact as a function of the peak stimulus current, both measured and simulated. Three measured traces taken from different electrodes give a feel for the variation to be expected from nominally-identical electrodes. The difference in magnitudes between the simulated and measured traces is attributed to the ideal nature of the compact model, within which all electrodes are identical and common-mode signals have no contribution. In the circumstances agreement is considered to be excellent.

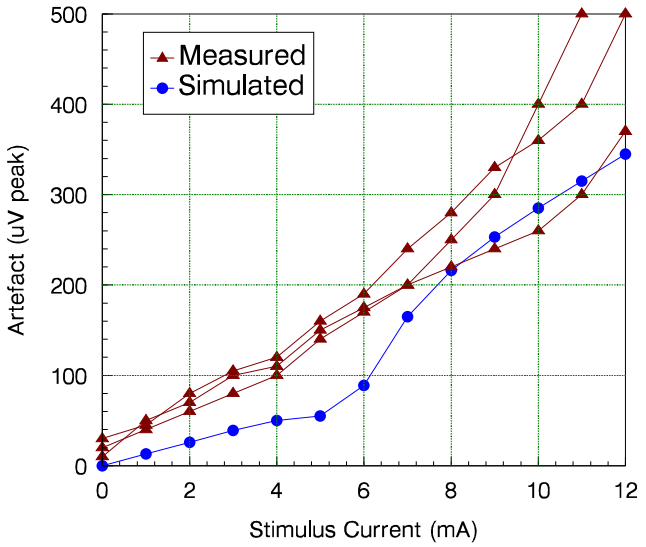

Fig. 9. Magnitude of the decaying artefact, measured and simulated, plotted against peak stimulus current. The three measured traces represent the normal variation between supposedly-identical leads. Note the zero-offset on measured traces resulting from common-mode and switching signals.

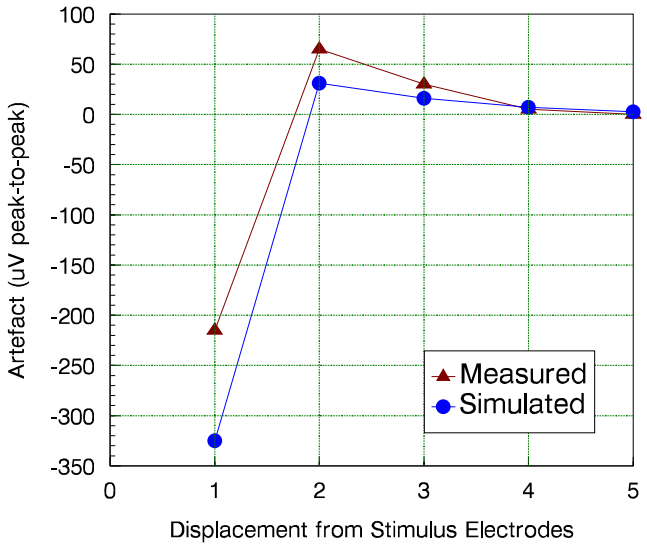

Fig. 10. Measured and simulated magnitude of artefact measured between adjacent electrodes as a function of their displacement along a lead, measured in units of "electrode spacing", 7 mm in our case. An offset at zero stimulus current of about 20μV has been subtracted from measured data.

Figure 10 presents measurement and prediction of the artefacts measured between adjacent electrode pairs v(3,4), v(4,5), v(5,6), v(6,7), and v(7,8). As usual, a stimulus of 5mA is applied at electrode 2 with ground return through electrode 1. The simulation predicts the paradoxical change in sign of the artefact between the first and second electrode pairs. This lends considerable confidence to the veracity of the model.

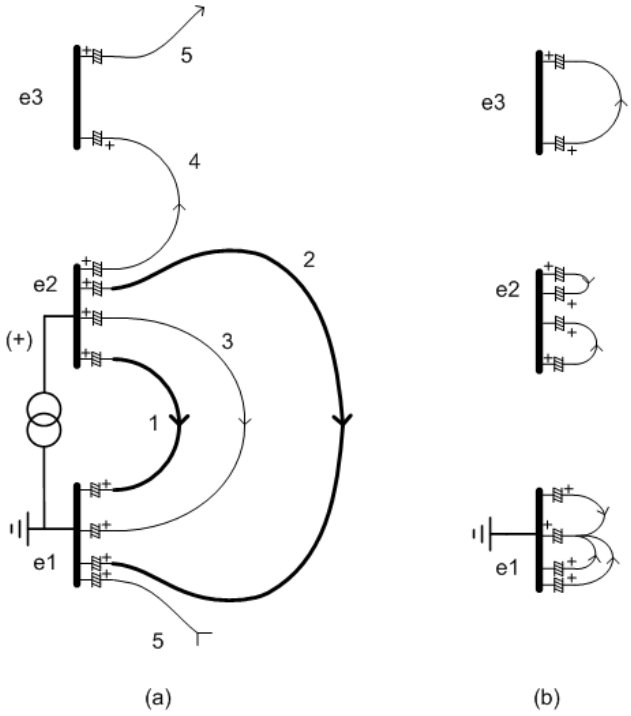

Fig. 11. Diagram of current flow paths in the simplified case of two stimulating and one passive electrode, during (a) and then after (b) the pulse.

IV. Analysis and Conclusion

The impact of charges "passively displaced" by flowing stimulus currents cannot be underestimated. These displaced charges are inescapable. To emphasise this point and aid understanding, consider figure 11. The current labelled "5" may be 100 times smaller than "1", "2", and "3", but it leaves e3 with significant displaced charge. This diagram suggests how a completely passive metal structure—potentially quite disconnected from the electrode assembly—becomes "charged", that is how it comes to host a displaced population of mobile species in the Gouy-Stern-Chapman layer. Figures 12 and 13 then show the impact on residual field of including or omitting a single cuff. Comparison of these two figures quickly reveals that an added piece of metal introduces new regions where the field changes polarity, passing through zero, where there was before no zero at all. Of course, this phenomenon will occur with any metallic structure in proximity of the stimulating electrodes, not only components of the implanted lead itself.

It has been a long-standing conjecture that uneven charge distribution on the surface of individual electrodes contributes to the long pulse tails referred to as "artefacts" and observed on implanted measurement electrodes. We assert that the observation that our electrode model only predicts artefacts at all when the electrode is modelled as a parallel series of "slices" that are free to accumulate unequal charges confirms the conjecture. We also assert that the model shows surface charge imbalance to be the main or possibly sole contributor; the model can account for the magnitude of artefacts observed in a well-designed implant with good CMRR in the FEA.

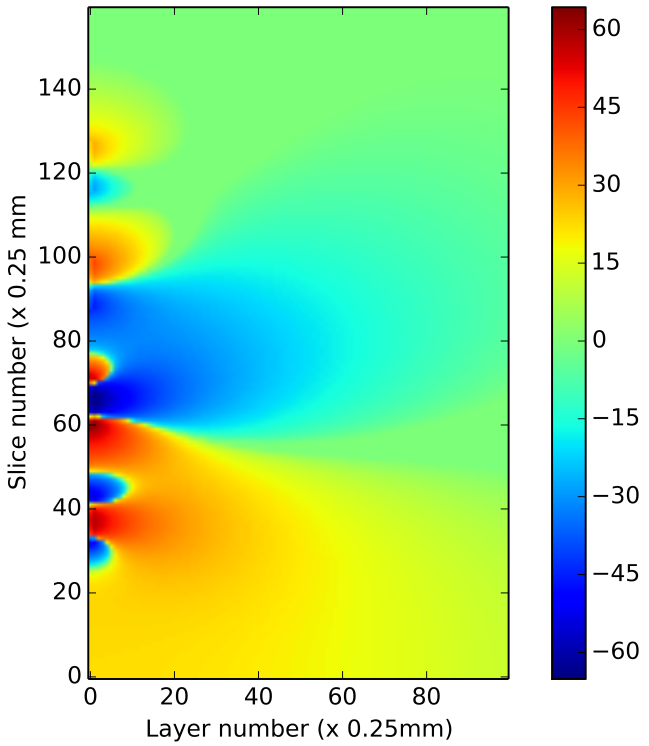

Fig. 12. Plot of electric field in the saline surrounding a set of electrodes shortly after removal of stimulus, for two stimulating and two passive electrodes. The electrodes are placed along the y-axis. The electrodes are completely disconnected, so that no current flows into or out of the electrolyte.

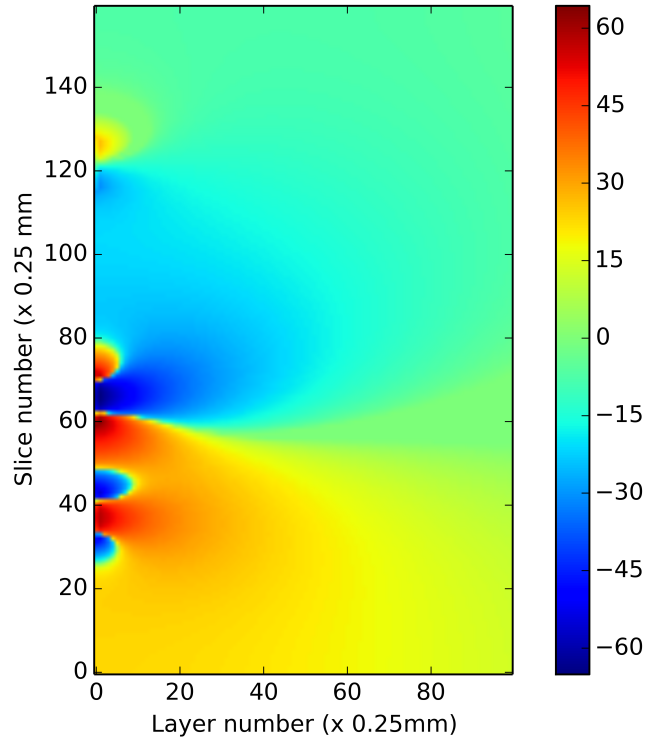

Fig. 13. Plot of electric field in the saline surrounding a set of electrodes shortly after removal of stimulus, for two stimulating and one passive electrodes; in comparison with figure 12 electrode e3 has been removed.

As far as the authors are aware, this is the first confirmation of an electrode-intrinsic mechanism responsible for electrode artefacts. By "electrode-intrinsic" we mean a phenomenon that is an inescapable physical consequence of the electrode design, inherent to the geometry and materials of the electrode, and independent of electrical action, connection, or loading of associated electronics.

We have shown that measured artefact is the sum of several independent components, with at least one from each involved electrode contact. The final measured artefact, being the sum of essentially-opposing contributions, is very sensitive to variations in their magnitudes. This goes a long way towards explaining the variation in artefact observed by clinicians.

Electrical efforts to minimise artefact tails in neuromodulation systems are important and ongoing. [13] We observe that the artefact mechanism identified in this manuscript arises within the electrode-electrolyte system itself, all external electronic influences being negligibly small. Even a perfect FEA will encounter this signal.

Acknowledgement

The authors would like to acknowledge Saluda Medical and John Parker for their valuable support. Dr Mark Bickerstaff assisted with implant hardware and firmware, and Dominic Greco provided mechanical support.

References

[1] Scott Stanslaski, Pedram Afshar, Peng Cong, Jon Giftakis, Paul Stypulkowski, Dave Carlson, Dave Linde, Dave Ullestad, Al-Thaddeus Avestruz, and Timothy Denison, "Design and Validation of a Fully Implantable, Chronic, Closed-Loop Neuromodulation Device With Concurrent Sensing and Stimulation", *IEEE Transactions on Neural Systems and Rehabilitation Engineering*, vol.20, no.4, 2012, pp.410–421.

[2] Peng Cong, Piyush Karande, Jonathan Landes, Rob Corey, Scott Stanslaski, Wes Santa, Randy Jensen, Forrest Pape, Dan Moran, and Tim Denison, "32-channel modular bi-directional neural interface system with embedded DSP for closed-loop operation", *40th European Solid State Circuits Conference* (ESSCIRC), 2014, pp.99–102.

[3] Mark J. Connolly, Robert E. Gross, and Babak Mahmoudi, "Towards a platform for prototyping control systems for optimization of neuromodulation therapies", *IEEE Biomedical Circuits and Systems Conference* (BioCAS), 2015, pp.1–4.

[4] Kevin C. McGill, Kenneth L. Cummins, Leslie J. Dorfman, Bruno B. Berlizot, Kelly Luetkemeyer, Dwight G. Nishimura, and Bernard Widrow, "On the Nature and Elimination of Stimulus Artifact in Nerve Signals Evoked and Recorded Using Surface Electrodes", IEEE Transactions on Biomedical Engineering, Vol. BME-29, No. 2, February 1982.

[5] Virginie Attina, Faten Mina, Pierre Stahl, Yvan Duroc, Evelyne Veuillet, Eric Truy, and Hung Thai-Van, "A new method to test the efficiency of Cochlear Implant artifacts removal from Auditory Evoked Potentials", IEEE Transactions on Neural Systems and Rehabilitation Engineering, 2017.

[6] Zhijun Zhou and Paul A. Warr, "A High Input Impedance Low Noise Integrated Front-End Amplifier for Neural Monitoring", *IEEE Transactions on Biomedical Circuits and Systems*, vol.10, no.6, 2016, pp.1079–1086.

[7] Jonathan Scott and Peter Single, "Compact Nonlinear Model of an Implantable Electrode Array for Spinal Cord Stimulation (SCS)", IEEE Transactions on Biomedical Circuits and Systems, vol.8, no.3, pp.382–390, 2014.

[8] Mark H. Jones and Jonathan Scott, "Scaling of Electrode-Electrolyte Interface Model Parameters In Phosphate Buffered Saline", IEEE Transactions on Biomedical Circuits and Systems, vol.9, no.3, pp.441–448, 2015.

[9] David K Money, Chief Scientist, Cochlear Limited, private communication, 2000.

[10] A. V. Delgado, F. Gonzlez-Caballero, R. J. Hunter, L. K. Koopal, and J. Lyklema, "Measurement and Interpretation of Electrokinetic Phenomena", *Pure and Applied Chemistry*, Vol. 77, No. 10, pp. 1753–1805, 2005.
[11] St. Jude Medical (now Abbott), "Octrode Percutaneous Lead for Neuromodulation", specifications available on the internet at https://www.sjm.com/en/professionals/resources-and-reimbursement/technical-resources/chronic-pain-therapies/spinal-cord-stimulation/percutaneous-leads/octrode-leads, retrieved April 2017.
[12] Evoke 12C Percutaneous Leads, Saluda Medical, specifications available in the "Evoke Surgical Guide", version 6, http://www.saludamedical.com/manuals/, retrieved May 2017.
[13] E. J. Peterson, D. A. Dinsmoor, D. J. Tyler and T. J. Denison, "Stimulation artifact rejection in closed-loop, distributed neural interfaces", ESSCIRC, 42nd European Solid-State Circuits Conference, Lausanne, 2016, pp. 233-236.

Peter Single is the Chief Technology Officer at Saluda Medical Pty Ltd, where he is responsible for the neurostimulation implant and the techniques for measuring evoked responses. He graduated with an Electrical Engineering degree from The University of Sydney in 1978. He was an IC designer for National Semiconductor in Sunnyvale from 1980 to 1984, and Austek Microsystems Pty Ltd in Adelaide, South Australia, from 1985 to 1990. He was a systems engineer at Cochlear Pty Ltd from 1991 to 2002. From 2002 to 2006 he worked for G2 Microsystems Pty Ltd.

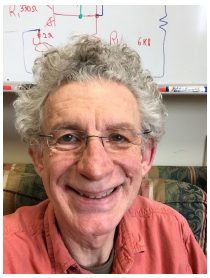

Jonathan Scott (M'80–SM'99) is the Foundation Professor in Electronic Engineering at the University of Waikato, Hamilton, New Zealand. From 1998 to 2006 he was with the Hewlett-Packard and Agilent Technologies Microwave Technology Center in Santa Rosa, California, where he was responsible for advanced measurement systems. In 1997 and 1998 he was Chief Engineer at RF Technology in Sydney. He was with the University of Sydney in the Department of Electrical Engineering prior to 1997. Professor Scott holds five degrees, has authored over 150 refereed publications, several book chapters and a textbook, and he holds more than a dozen patents, several licensed or covering active products. Professor Scott's educational interests include Threshold Concepts and their application, particularly across engineering disciplines.